A Constitutive Model for Overconsolidated Clay based on the Hardening State Parameter

ADVANCED SOIL MODELS

Last Updated: December 13, 2019

Table of Contents

1 Introduction

Natural deposits are often characterized by a given degree of over-consolidation resulting from a wide range of geological processes and human activities (erosion, melting of glaciers, cyclic loading, water table variations, etc). Their presence in highly populated urban areas may have an important effect on the geotechnical design of structures like foundations, tunnels and excavations. From a modelling standpoint, although the formulation of the Original and Modified Cam-Clay model (*MCC*) explains the fundamental mechanisms of normally consolidated clays, the applicability of these constitutive theories to simulate the behaviour of Over-Consolidated Clays (*OCC*) show a limited model performance due to:

- The existence of a large elastic region.
- A quick transition from the elastic to plastic regime.
- An inadequate prediction of the peak stress and dilatancy on the dry side (i.e., the so-called supercritical region).

Compared with normally consolidated clays, over-consolidated clays are characterized by a lower void ratio, a higher strength stress and exhibit a stress dilatancy in combination with strain softening failure during the post-peak regime (Yao et al., 2008 (on page 38)).

To fill this gap, several formulations have been proposed in the past to better capture the salient features of an *OCC* deposit (Pender, 1978; Hueckel et al., 1992; Whittle, 1993; Mita et al., 2004; Yao et al. 2009; Gao et al., 2017; Chen and Yang, 2017; Sternik, 2017 (on page 37)). Recently, a model using a state parameter as a fundamental variable to characterize the consolidation process of a clay has been implemented by Jockovic and Vukicevic (2017) (on page 37) to mimic the behavior of *OCC*, thus showing the applicability of this approach for this class of materials. Specifically, the framework of critical state mechanics has been combined within a bounding surface approach through the definition of a state parameter.

Hereafter, a PLAXIS implementation of the HArdening State Parameter (*HASP*) model (Jockovic and Vukicevic, 2017 (on page 37)) is presented to show the capability of these constitutive equations in simulating laboratory experiments on *OCCs*. To improve the model performance, the Small-Strain Overlay model (Benz, 2007 (on page 37)) is integrated in the *HASP* framework to better capture the non-linear degradation of the shear properties which are crucial to evaluate the deformability of geotechnical structures. After the material calibration, some practical problems solved with the *HASP* model and PLAXIS 2D/3D code are also presented.

Mathematical Notation

It is common practice in geomechanical modeling to express the stress dependency of the yield and plastic potential surfaces as a function of stress invariants, i.e., the mean stress p, the stress deviator q and the Lode's angle θ. They are defined as:

$$\begin{cases} p = \dfrac{tr(\sigma)}{3} = \dfrac{\sigma_{ij}\delta_{ij}}{3} = \dfrac{\sigma_{xx} + \sigma_{yy} + \sigma_{yy}}{3} \\ q = \sqrt{\dfrac{3}{2}(s_{ij}s_{ij})} = \sqrt{\dfrac{3}{2}}\|s\| \\ \theta = \dfrac{1}{3}\arcsin\left[\sqrt{6}\left(\dfrac{tr(s^3)}{tr(s^2)^{3/2}}\right)\right] \end{cases}$$

where

s_{ij}	=	Deviator component of the stress state (i.e., $s_{ij} = \sigma_{ij} - p{\cdot}\delta_{ij} \rightarrow \delta_{ij}$ is Kronecker's symbol)
$tr(\cdot)$	=	Trace that gives the sum of the diagonal terms of the matrix (i.e., $\text{tr}(\sigma_{ij}) = \sigma_{xx} + \sigma_{yy} + \sigma_{xx} + \sigma_{zz} = 3P$).

A general representation of the stress deviator and its norm is reported as:

$$s_{ij} = \begin{bmatrix} \sigma_{xx} - p & \sigma_{xy} & \sigma_{xz} \\ \sigma_{yx} & \sigma_{yy} - p & \sigma_{yz} \\ \sigma_{zx} & \sigma_{zy} & \sigma_{zz} - p \end{bmatrix}$$

$$\|s\| = (\sigma_{xx} - p)^2 + (\sigma_{yy} - p)^2 + (\sigma_{zz} - p)^2 + 2\left(\sigma_{xy}^2 + \sigma_{zy}^2 + \sigma_{zx}^2\right)$$

Analogously, similar quantities are defined also for the strain tensor ε_{ij}:

$$\begin{cases} \varepsilon_v = \varepsilon_{xx} + \varepsilon_{yy} + \varepsilon_{zz} \\ \varepsilon_q = \sqrt{\dfrac{2}{3}\left(\varepsilon_{s_{ij}}\varepsilon_{s_{ij}}\right)} = \sqrt{\dfrac{2}{3}}\|\varepsilon_s\| \end{cases}$$

where

ε_v	=	Volumetric strain.
$\varepsilon_{s_{ij}}$	=	strain deviator. Defined as: $\varepsilon_{s_{ij}} = \varepsilon_{ij} - (\varepsilon_v \cdot \delta_{ij}) / 3$.

$$\varepsilon_{s_{ij}} = \begin{bmatrix} \varepsilon_{xx} - \varepsilon_v/3 & \varepsilon_{xy} & \varepsilon_{xz} \\ \varepsilon_{yx} & \varepsilon_{yy} - \varepsilon_v/3 & \varepsilon_{yz} \\ \varepsilon_{zx} & \varepsilon_{zy} & \varepsilon_{zz} - \varepsilon_v/3 \end{bmatrix}$$

$$\|\varepsilon_s\| = \left(\varepsilon_{xx} - \frac{\varepsilon_v}{3}\right)^2 + \left(\varepsilon_{yy} - \frac{\varepsilon_v}{3}\right)^2 + \left(\varepsilon_{zz} - \frac{\varepsilon_v}{3}\right)^2 + 2\left(\varepsilon_{xy}^2 + \varepsilon_{zy}^2 + \varepsilon_{zx}^2\right)$$

For triaxial stress paths ($\sigma_{xx} = \sigma_{yy} < \sigma_{zz}$, $\sigma_{xz} = \sigma_{xy} = \sigma_{yz} = 0$), the general definition of invariants can be simplified as:

$$p = (\sigma_{zz} + 2\sigma_{xx})/3 \qquad q = |\sigma_{zz} - \sigma_{xx}|$$

$$\varepsilon_v = (\varepsilon_{zz} + 2\varepsilon_{xx})/3 \qquad \varepsilon_q = 2|\varepsilon_{zz} - \varepsilon_{xx}|/3$$

In this context, the deviatoric and volumetric plastic strain are computed as:

$$\dot{\varepsilon}_v^p = \dot{\Lambda}\left(\frac{\partial g}{\partial p}\right); \quad \dot{\varepsilon}_v^p = \dot{\Lambda}\left(\frac{\partial g}{\partial q}\right)$$

Hereafter, a positive compression convention will be adopted by following the usual soil mechanics framework.

2
General Framework

The mechanical response of over-consolidated soils is strongly influenced by the loading history of the deposit which characterizes the initial conditions of the soil and the resulting stress-strain behaviour. The unloading/ reloading process due to the former presence of a Pre-Overburden Pressure (i.e., *POP*) modifies the stress path as depicted in *Figure 1*. This variable is defined as:

$$POP = \sigma_v^{',max} - \sigma_v^{'} \qquad Eq.\ [1]$$

where

$\sigma_v^{'}$ = Vertical effective stress in the soil.

$\sigma_v^{',max}$ = Maximum value due to pre overburden pressure.

It is common practice in soil mechanics to evaluate the degree of consolidation of a clay also by considering the over-consolidated ratio (*OCR*) which is defined as the ratio between the maximum and current distribution of the vertical effective stress:

$$OCR = \sigma_v^{',max} / \sigma_v^{'} \qquad Eq.\ [2]$$

According to the specific value of the *OCR* it is possible to classify the conditions of the soil as:

- Normally consolidated (*OCR* =1)
- Over-consolidated (1<*OCR*<10)
- Highly over-consolidated (*OCR*>10)

Commonly determined with the strategy proposed by Casagrande (1936) (on page 37), the degree of over consolidation can result from different situations:

- Removal/reduction of mechanical loads due to natural processes like erosion of the ground surface or elimination of ice sheets in glacier zones.
- The variation of the water table (*WT*) position which can induce changes in the effective stress field, thus implying a possible consolidation of the soil. This process is explained by considering that a drop of the *WT* makes the effective stresses increasing. The subsequent rise of the *WT* results to a reduction of the effective stresses, thus having a lower tensional level within the ground compared to the values which have been reached in former stress path of the soil.
- Preloading stages can be employed in the geotechnical practice to limit the soil deformability which can be excessive for a structure. This is usually carried out with a soil fill. The applied overload must be equal or, preferably, higher than the tension increase transmitted to the ground by the load of the structure or the final fill. Using this method, it is possible to reduce the settlement of the structure compared to the one which might have taken place without the application of the preload. As a result, it provides an over-consolidation of the ground, thus reducing also additional settlements associated with secondary consolidation.

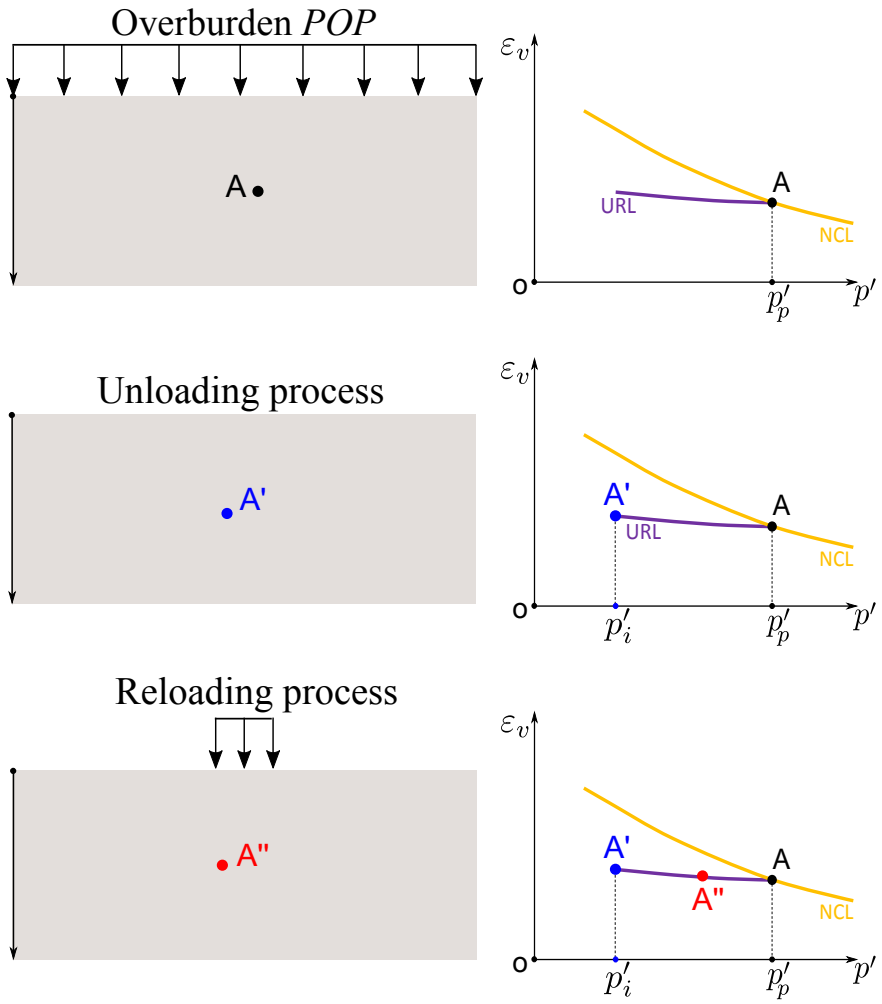

Figure 1: Schematic representation of the stress path resulting from an over-consolidation process

The mechanical behaviour of normally and over consolidated clays is depicted in *Figure 2* which emphasizes the salient differences of the stress-strain paths resulting from experiments in drained and undrained conditions. By observing this figure, it is readily apparent that *OCCs* are characterized by a higher stress at critical state (i.e., the undrained strength, point E of *Figure 2*) if compared with the same stress path in drained condition. At variance with normally consolidated clays which exhibit a contractive behaviour during shearing, *OCCs* show a remarked tendency to dilate during shearing which is often accompanied with the development of shear bands during the post-peak behaviour.

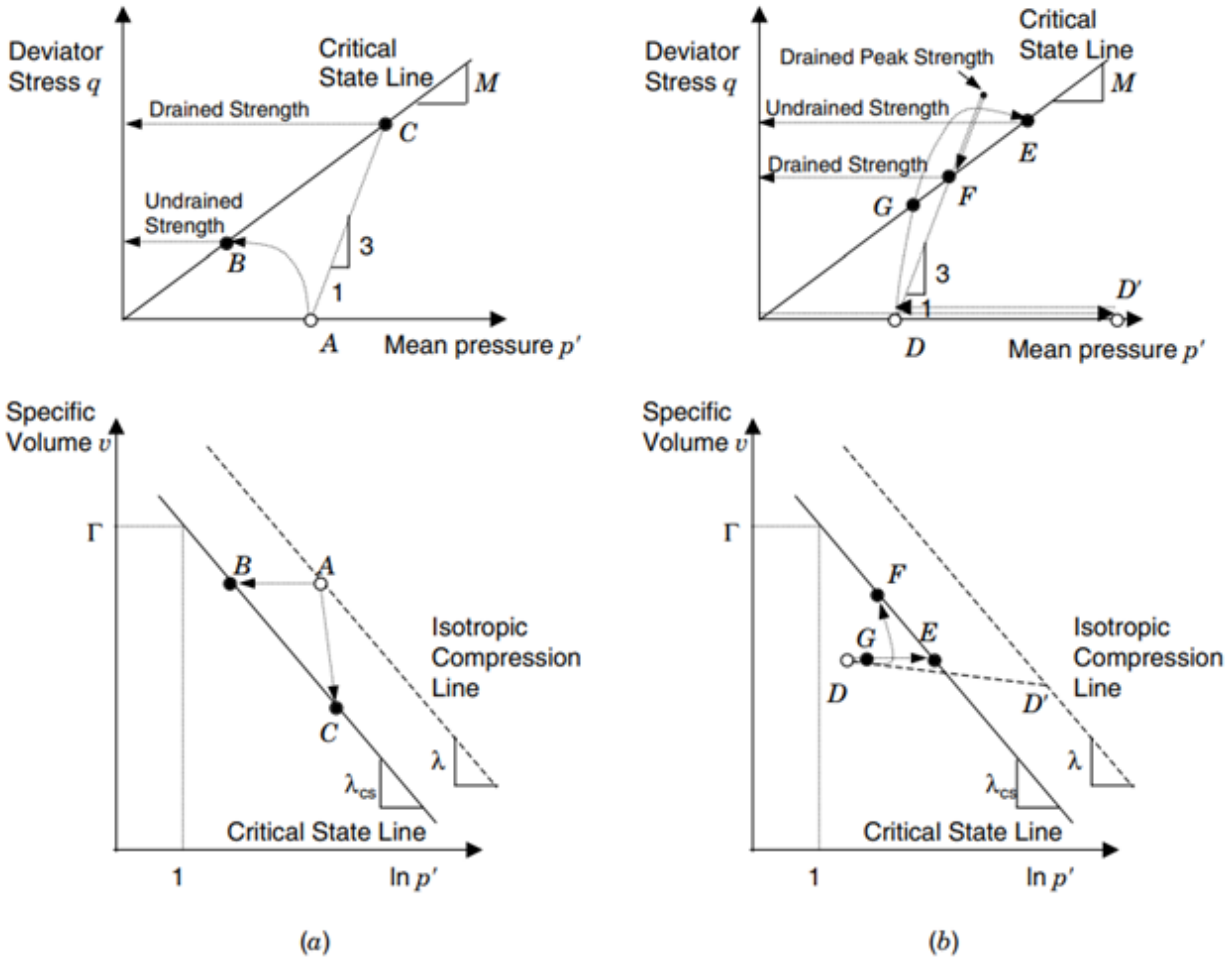

Figure 2: Drained and undrained stress-strain response using the critical state concept for (a) Normally Consolidated Clays and (b) Over-Consolidated Clays (figure rearranged by Mitchell and Soga, 2005)

3 Constitutive Equations

Critical State Framework

Consistently with the constitutive models implemented in PLAXIS code, the slope of the *CSL/NCL* (i.e., the Critical State Line and Normal Consolidated Line) and the *URL* (i.e., the parameters λ and κ) have been rescaled to replace the current void ratio *e* with the volumetric strain ε_v.

$$\lambda^* = \lambda / \left(1 + e_i^{ref}\right), \quad \kappa^* \approx \kappa / \left(1 + e_i^{ref}\right) \qquad Eq.\ [3]$$

where

e_i^{ref} = Initial void ratio of the soil considered as a reference to calculate the elastic properties of the model.

λ^* and κ^* = Rewritten by using the compression and swelling indexes $\lambda^* = C_c / 2.3$ and $\kappa^* = 2 \cdot C_s / 2.3$.

By using this convention, the *CSL* can be redefined as:

$$\varepsilon_v = \varepsilon_\Gamma - \lambda^* \cdot In\left(p'\right) \qquad Eq.\ [4]$$

In which ε_Γ is equal to the volumetric strain corresponding to *1kPa.* This equation can be expressed also by considering p'_0 as a reference mean stress (*Figure 3*)) :

$$\varepsilon_v - \varepsilon_v^0 = -\lambda^* \cdot In\left(p' / p'_0\right) \qquad Eq.\ [5]$$

or for the unloading/reloading line:

$$\varepsilon_v - \varepsilon_v^0 = -k^* \cdot In\left(p' / p'_0\right) \qquad Eq.\ [6]$$

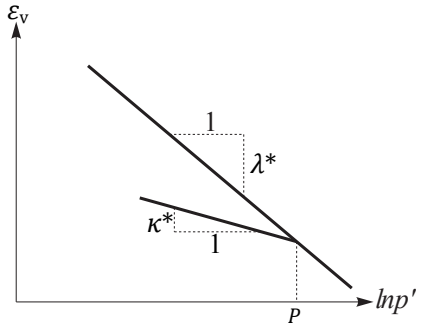

Figure 3: NCL and URL in ε_v- ln (p') plane

Hasp model

In *HASP* formulation the elastic domain is defined through the elliptic surface of the Modified Cam-Clay model which is also considered to define the bounding surface of this model (i.e., the elastic domain in the former stage of consolidation, *Figure 4*):

$$f = \frac{q^2}{M^2} + p'\left(p' - p_0'\right) \qquad Eq.\ [7]$$

where

M	=	Gradient of the critical state line in q-p' plane.
p_0	=	Size of the current yield surface (i.e., the initial pre-consolidation pressure in isotropic conditions).

The equation *Eq. [7]* can be rewritten also as a function of the stress ratio $\eta=q/p'$:

$$\left(\frac{\eta^2 + M^2}{M^2}\right) = \frac{p_0'}{p'} \qquad Eq.\ [8]$$

The dependency on the Lode angle θ is introduced in this model through the relation proposed by Van Eekelen (1980) (on page 37) :

$$M(\theta) = a \cdot [1 + b \cdot sin(3\theta)]^n \qquad Eq.\ [9]$$

In which a and b are expressed as a function of the reduced radius in compression and extension, respectively, (i.e., r_C and r_E):

$$a = \frac{r_C}{(1+b)^n} \quad , \quad b = \frac{\left(\frac{r_C}{r_E}\right)^{1/n} - 1}{\left(\frac{r_C}{r_E}\right)^{1/n} + 1} \qquad Eq.\ [10]$$

The reduced ratios are defined with the friction angles in extension and compression:

$$r_C = \frac{1}{\sqrt{3}} \cdot \left(\frac{2 \cdot sin\phi_C}{3 - sin\phi_C}\right),\ r_E = \frac{1}{\sqrt{3}} \cdot \left(\frac{2 \cdot sin\phi_E}{3 + sin\phi_E}\right) \qquad Eq.\ [11]$$

For the sake of simplicity, both the friction angles are enforced to be equal to the corresponding value at critical state (i.e., $\phi_E \equiv \phi_C \equiv \phi_{cv}$), while the exponent n is prescribed to be equal to n=-0.229, thus guaranteeing the convexity of the yield surface for values of friction angle commonly employed in geotechnical engineering problems Van Eekelen (1980) (on page 37).

To introduce a measure of the current state of the soil in relation to its density and the corresponding stress, a state parameter ψ is defined to track the distance between the *URL* and the *CSL*:

$$\psi = v + \lambda \cdot ln\, p' - \Gamma \qquad Eq.\ [12]$$

In this equation v is the specific volume, Γ is the specific volume on the *CSL* for a reference pressure of *1 kPa* while λ is the slope of the normal compression line. In this manner, for highly over-consolidated clays the sign of the state parameter is negative (i.e., ψ<0), while for normally consolidated clay is positive (ψ>0). In both cases, when the stress state tends to approach the critical state line, the state parameter tends to vanish (i.e., ψ=0). A sketch of the yield and bounding surface is presented in *Figure 4*, where the stress states A and $\bar{A}$ refers to the

current stress and the conjugate stress point, respectively (i.e., the map of the current stress on the bounding surface by assuming the origin of the *q-p'* axes as a centre of projection).

As detailed in Jockovic and Vukićević (2017) (on page 37) , it is possible to express the state parameter with respect to the bounding surface as a function of the current stress ratio $\eta=q/p'$:

$$\bar{\psi} = (\lambda - \kappa) \cdot \ln\left(\frac{2\,M^2}{M^2 + \eta^2}\right) \qquad Eq.\ [13]$$

In the *HASP* formulation, both the state parameters ψ and $\bar{\psi}$ play a central role in the plastic flow and the corresponding hardening process. Consistently with the notation reported in the previous section, the state parameters will be reported with the symbol * as they will be expressed by using λ^*, κ^* and ε^* (i.e., ψ^* and $\bar{\psi}^*$):

$$\psi^* = \varepsilon_v + \lambda^* \cdot \ln(p') - \varepsilon_\Gamma \qquad Eq.\ [14]$$

$$\bar{\psi}^* = (\lambda^* - \kappa^*) \cdot \ln\left(\frac{2\,M^2}{M^2 + \eta^2}\right) \qquad Eq.\ [15]$$

Although characterized by a different notation, ψ^* and $\bar{\psi}^*$ have the same geometrical meaning of ψ and $\bar{\psi}$ with the only difference that the distance between the *URL* and *CSL* is reported in the plane ε_v - *ln(p')*.

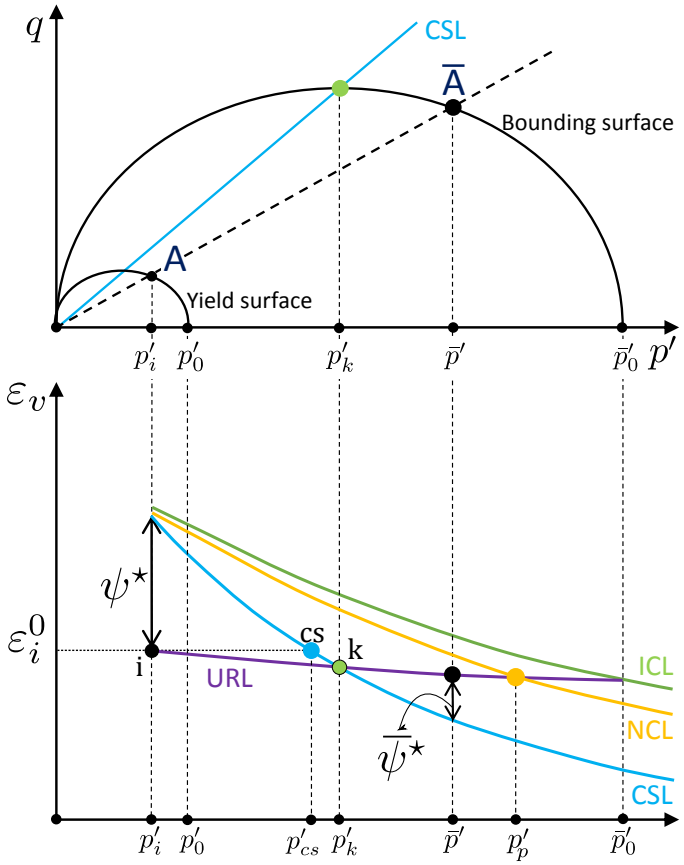

Figure 4: Schematic representation of the theoretical framework used in HASP model including the current stress A and its conjugate point $\bar{A}$ (figure after Jockovic & Vukicevic, 2017)

Plastic flow and hardening rule

The volumetric hardening rule employed in the former formulation of Modified Cam-Clay model is unable to develop negative dilatancy before the peak strength and to simulate the transition from contractive to dilatant behaviour. For this purpose, a generalized hardening rule expressed also as a function of the plastic shear strain has been considered in the former contribution by Nova and Wood (1979) (on page 37) and Nova (2007) :

$$dp_0' = \frac{v p_0'}{\lambda - \kappa}\left(d\varepsilon_v^p + \xi d\varepsilon_q^p\right) = \frac{v p_0'}{\lambda - \kappa} d\varepsilon_v^p \left(1 + \frac{\xi}{d}\right) = \left(\frac{v p_0'}{\lambda - \kappa}\right) \cdot d\varepsilon_v^p \cdot \omega \qquad Eq.\ [16]$$

where

d = Dilatancy function (i.e., the ratio $d = d\varepsilon_v^p / d\varepsilon_q^p$).

ω = Hardening coefficient of the *HASP* model, expressed as a function of the state parameters $\bar{\psi}^*$ *and* ψ^*, thus enabling to simulate a positive/ negative dilation according with the position of the stress state with respect to the *CSL*:

$$\omega = \left(1 + \frac{\bar{\psi}^* - \psi^*}{\bar{\psi}^*}\right) \cdot R \cdot h \qquad Eq.\ [17]$$

where

R = Isotropic over-consolidation ratio which is defined as the ratio between $\bar{p}_0'$ and the current mean effective stress p' (i.e., $R = \bar{p}' / p' = \bar{p}_0' / p'$).

h = Additional parameter implemented in the model (See Parameter h (on page 24)).

From a general perspective, the model formulation is characterized by an associated flow rule, therefore, the same equation of the yield criterion is employed for the plastic potential:

$$d\varepsilon^p = \Lambda\left(\frac{\partial f}{\partial \sigma}\right) \qquad Eq.\ [18]$$

where

Λ = Increment of the plastic multiplier.

Specifically, the plastic characteristics of the model in terms of strain invariants are computed as:

$$d\varepsilon_v^p = \frac{\lambda - \kappa}{v p'}\left[\left(\frac{M^2 - \eta^2}{M^2 + \eta^2}\right)dp' + \left(\frac{2\eta}{M^2 + \eta^2}\right)dq\right]\frac{1}{\omega} \qquad Eq.\ [19]$$

$$d\varepsilon_q^p = \frac{\lambda - \kappa}{v p'}\left[\left(\frac{2\eta}{M^2 + \eta^2}\right)dp' + \left(\frac{4\eta^2}{(M^2 + \eta^2)(M^2 - \eta^2)}\right)dq\right]\frac{1}{\omega} \qquad Eq.\ [20]$$

In the presented formulation, the effective stress is not allowed to go in tension. It is worth remarking that, according to the *HASP* model, the stress paths starting from a former unloading stage are characterized by a plastic behaviour from the beginning of the reloading. This scenario is depicted in *Figure 5 (a)* in which the size of the yield surface is updated according to the value of the stress state in *B* (i.e., P_0' is updated to $P_0'^{,ur}$), thus enabling to reach the stress state *C* through a plastic response. This particular case differs with the elasto-plastic theory which predicts an elastic response when the stress state is within the yield surface (*Figure 5 (b)*). In the current implementation of the *HASP* model both ways to simulate a stress path during a reloading stage are considered and they can be selected through a flag input which enables to choose a plastic or an elastic reloading.

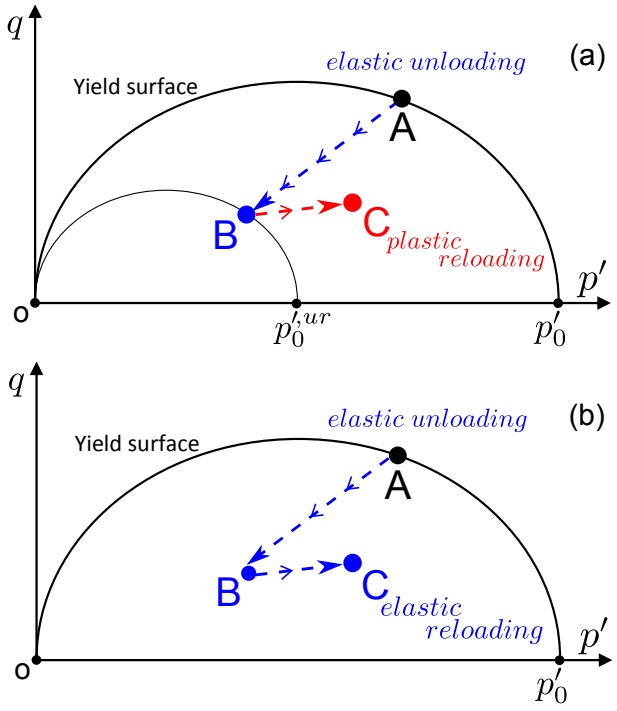

Figure 5: Schematic representation of the unloading behavior according to (a) the formulation of Jockovic and Vukićević (2017) (i.e., the yield surface is updated in the reloading stage, thus enabling the response in reloading to be plastic from the beginning of the loading) and (b) the elasto-plastic theory which considers the behaviour to be elastic when the stress state is within the yield surface.

Elastic stiffness

The isotropic characteristics of the elastic stiffness are expressed through the elastic relation linking the bulk modulus K_{ur} and shear modulus G_{ur} with the Young modulus E_{ur} and Poisson's ratio ν_{ur} :

$$K_{ur} = \frac{E_{ur}}{3\,(1 - 2\nu_{ur})}, \quad G_{ur} = \frac{3\,K_{ur}\,(1 - 2\nu_{ur})}{2\,(1 + \nu_{ur})} \qquad Eq.\ [21]$$

By considering the pressure-dependent characteristics of the Young modulus, K_{ur} can be rearranged as:

$$E_{ur} = E_{ur}^{ref}\left(\frac{p'}{p_{ref}}\right), \; K_{ur} = \frac{p'}{\kappa^*} \qquad Eq.\ [22]$$

where

p_{ref}	=	Reference value of the mean pressure.
E_{ur}^{ref}	=	Reference value of the Young modulus.

To include in the model the possibility of simulating the degradation of the elastic properties from very small strain (*Figure 6*) , the Small Strain Overlay (*SSO*) model proposed by Benz (2007) (on page 37) is included in the implementation of the *HASP* model. According to this approach, the shear modulus degradation is expressed as:

$$G_t = \frac{G_0}{\left[1 + 0.385 \cdot \left(\frac{\gamma_{hist}}{\gamma_{0.7}}\right)\right]^2} \qquad Eq.\ [23]$$

where

G_t	=	Tangent shear modulus.
G_0	=	Initial shear modulus at very small strain
γ_{hist}	=	Represents a projection of the strain history into the current loading direction (for more details on how to compute γ_{hist} (see Benz, 2007 (on page 37)) .
$\gamma_{0.7}$	=	Shear strain level at which the secant shear modulus G_s is reduced to about 70% of G_0.

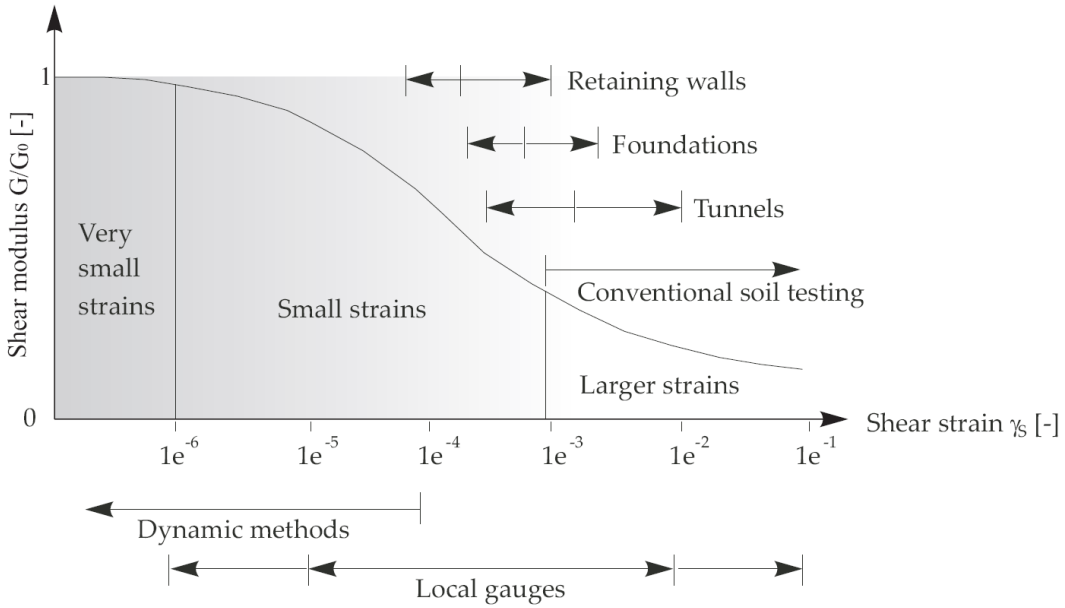

Figure 6: Characteristic stiffness-strain behaviour of soil with typical strain ranges for laboratory tests and structures (after Atkinson and Sallfors (1991))

Consistently with pressure-dependent characteristics of the Young modulus, the initial shear modulus is also implemented with a similar expression:

$$G_0 = G_0^{ref}\left(\frac{p'}{p_{ref}}\right) \qquad Eq.\ [24]$$

The small-strain stiffness reduction is bounded by a certain lower limit determined by conventional laboratory tests. For this reason, the lower cut-off of the tangent shear modulus G_t is introduced through the unloading/ reloading stiffness G_{ur} which is defined in Eq. 21. In other words, if $G_t \geq G_{ur}$ then G_t=G_{ur}. More details on the use of small-strain stiffness can be found in PLAXIS **Material Models manual** within the section detailing the Hardening Soil model with small-strain stiffness (*HSsmall*).

4

Model Parameters and State Variables

Model Parameters

The model parameters presented in the previous section are further summarized in *Table 1*, where a short description of each parameter is provided. The presented model is characterized by a total of 9 material parameters, the value of the Pre-Overburden Pressure and a flag which enables to differentiate the response after unloading:

Table 1: List of material parameters

Parameter name	Short description	Unit
E_{ur}^{ref}	Reference unloading-reloading Young's modulus. It can be obtained from the unloading branch in a triaxial test with intermediate unloading stages. Given κ^*, p^{ref} and ν_{ur}, the parameter E_{ur}^{ref} can be calculated by using Eq. 25.	Stress
ν_{ur}	Poisson's ratio in unloading and reloading (elastic behaviour).	-
E_{oed}^{ref}	Reference oedometer modulus. It can be obtained from the primary loading branch in a one-dimensional compression test beyond the pre-consolidation stress. By knowing λ^* and p^{ref}, the parameter E_{oed}^{ref} can be calculated according to Eq. 25.	Stress
p^{ref}	Reference mean effective stress (used in stress-dependent stiffness calculations).	Stress
G_0^{ref}	Reference shear modulus at very small strains ($\varepsilon < 10^{-6}$) (Eq. 24). If G_0^{ref} or $\gamma_{0.7}$ is equal to 0.0 then the small-strain stiffness calculation is turned off.	Stress
$\gamma_{0.7}$	Threshold shear strain at which G_s=0.722G_0 (Eq. 24).	-
φ_{cs}	Friction angle at critical state.	degrees
K_0^{nc}	Earth pressure coefficient at rest. It is used to calculate the pre-consolidation state.	-

Parameter name	Short description	Unit
POP	Pre-Overburden Pressure. It is used to calculate the pre-consolidation state of the soil (Eq. 1).	stress
h	Parameter introduced to increase/decrease the plastic deformability of the soil.	-
elReload	Flag to switch from an elasto-plastic response during reloading paths (elReload=0), to an elastic behavior (*Figure 5*).	-

The parameter E_{ur}^{ref} and E_{oed}^{ref} can be calculated from the parameters p^{ref}, ν_{ur} and κ^* and λ^* as:

$$E_{ur}^{ref} = p^{ref}\left[\frac{3\left(1-2\,\nu_{ur}\right)}{\kappa^*}\right],\quad E_{oed}^{ref} = \left[\frac{p^{ref}}{\lambda^*}\right] \qquad Eq.\ [25]$$

while λ^*, κ^* can be derived from Eq. 3 . The description about how to determine small-strain stiffness parameters G_0^{ref} and $\gamma_{0.7}$ is given in detail in PLAXIS **Material Models manual** where a section dedicated to the Hardening Soil model with small-strain stiffness (*HSsmall* model). An example of the material parameters listed within PLAXIS graphical interface is shown in *Figure 7* . The model parameters reported in *Table 1* refers to the parameters used to model London Clay and their calculation will be detailed in the next section.

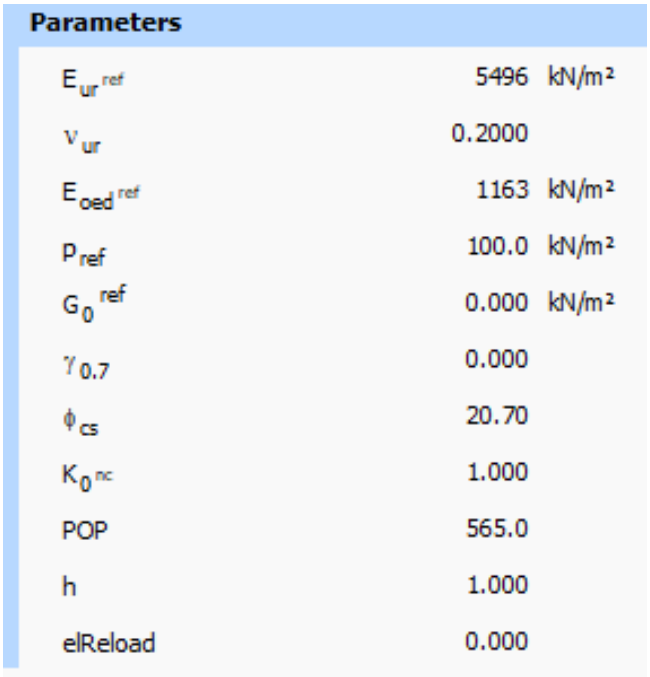

Figure 7: Model parameters of the HASP model in PLAXIS finite element

State Variables

Calculation of $p_p^{'}$ and ε_Γ

The parameters of K_0^{nc} and *POP* given by the user are used within PLAXIS to compute the pre-consolidation stress $p_p^{'}$ which is calculated internally in the model subroutines. At the beginning of a given analysis, or when **"Reset state variables"** checkbox is active in the **Phases window**, the mean effective stress and the deviator stress at pre-consolidation (i.e., $p_p^{'}$ and q_p respectively) are calculated, taking into account that $\sigma_{v0}^{'}$ prime is the initial effective vertical stress, using Eq. 26 and Eq. 27 :

$$p_p^{'} = \left[\frac{\left(\sigma_{v0}^{'} + POP\right) + 2 \cdot \left(\sigma_{v0}^{'} + POP\right) \cdot K_0^{\mathrm{nc}}}{3}\right] = \left(\sigma_{v0}^{'} + POP\right) \cdot \left[\frac{1 + 2 \cdot K_0^{\mathrm{nc}}}{3}\right] \qquad Eq.\ [26]$$

$$q_p = \left(\sigma_{v0}^{'} + POP\right) - \left(\sigma_{v0}^{'} + POP\right) \cdot K_0^{nc} = \left(\sigma_{v0}^{'} + POP\right) \cdot \left[1 - K_0^{\mathrm{nc}}\right] \qquad Eq.\ [27]$$

The corresponding stress ratio η_p can be calculated by using the definition reported in Eq. 28:

$$\eta_p = \frac{q_p}{p_p^{'}} = 3\left(\frac{1 - K_0^{nc}}{1 + 2K_0^{nc}}\right) \qquad Eq.\ [28]$$

If the initial pre-consolidation $p_p^{'}$ is known, the value of the *POP* can be calculated by inverting *Eq. 26*:

$$POP = p_p^{'}\left(\frac{3}{1 + 2K_0^{nc}}\right) - \sigma_{v0}^{'} \qquad Eq.\ [29]$$

The next variable required to integrate the model is the intercept of the critical state line with the ε_v-axis (i.e., the parameter ε_Γ), which is necessary to calculate the hardening variable ψ^* (see Eq. 14). The necessity to calculate ε_Γ is dictated by the fact that the reference deformation ε_i^0, resulting from the unloading process of the deposit, is initialized to zero and define the initial non-deformed configuration of the soil. Consistently with this assumption, the position of *CSL* has to move to keep the same relative distance between the *CSL* and *URL*, thus involving a new calculation of ε_Γ. For this reason, ε_Γ is not defined from the parameter Γ but it is recalculated by enforcing the value of ε_i^0 to zero:

$$\varepsilon_i^0 = \varepsilon_\Gamma - \lambda^* \cdot In\left(p_{cs}^{'}\right) = 0\ ,\ \ \varepsilon_\Gamma = \lambda^* \cdot In\left(p_{cs}^{'}\right) \qquad Eq.\ [30]$$

The value of $p_{cs}^{'}$ can be expressed as a function of the current mean stress $p_i^{'}$ by prescribing the following condition (see *Figure 8*):

$$\varepsilon_i^0 - \varepsilon_k = \lambda^* \cdot In(p_{cs}^{'} / p_k^{'}) = \kappa^* \cdot In(p_i^{'} / p_k^{'}) \qquad Eq.\ [31]$$

which can be rearranged as:

$$\frac{p_{cs}^{'}}{p_k^{'}} = \left(\frac{p_i^{'}}{p_k^{'}}\right)^{\frac{\kappa^*}{\lambda^*}},\quad p_{cs}^{'} = p_k^{'} \cdot \left(\frac{p_i^{'}}{p_k^{'}}\right)^{\frac{\kappa^*}{\lambda^*}} = p_k^{'\left(\frac{\lambda^* - \kappa^*}{\lambda^*}\right)} \cdot p_i^{'\left(\frac{\kappa^*}{\lambda^*}\right)} \qquad Eq.\ [32]$$

$p_k^{'}$ represents the intersection between the *CSL* and the *URL* as shown in *Figure 8*, which can be calculated by readapting Eq. 8 for the bounding surface:

$$\left(\frac{M^2}{\eta_p^2 + M^2}\right) = \frac{p_p^{'}}{\bar{p}_0^{'}} \qquad Eq.\ [33]$$

where $\bar{p}_0^{'}$ is the size of the bounding surface and is equal to $\bar{p}_0^{'} = 2p_k^{'}$. By using Eq. 33, it is possible to obtain:

$$p_k^{'} = \left(\frac{\eta_p^2 + M^2}{2M^2}\right) \cdot p_p^{'} \qquad Eq.\ [34]$$

The mean stress at critical state $p_{cs}^{'}$ can be written as a function the current mean stress $p_i^{'}$ and the mean stress at consolidation $p_p^{'}$:

$$p_{cs}^{'} = p_i^{'\left(\frac{\kappa^*}{\lambda^*}\right)} \cdot \left[p_p^{'} \cdot \left(\frac{\eta_p^2 + M^2}{2M^2}\right) \right]^{\left(\frac{\lambda^* - \kappa^*}{\lambda^*}\right)} \qquad Eq.\ [35]$$

By combining equation Eq. [34] and Eq. [30], it is possible to obtain an expression of ε_Γ as a function of stress state, as well as the undrained shear strength s_u, commonly employed in geotechnical design:

$$\varepsilon_\Gamma = \lambda^* \cdot In\left[\left(p_p^{'}\frac{\eta_p^2 + M^2}{2M^2}\right)^{\left(\frac{\lambda^* - \kappa^*}{\lambda^*}\right)} \cdot p_i^{'\left(\frac{\kappa^*}{\lambda^*}\right)}\right] \qquad Eq.\ [36]$$

$$q_{cs} = M\left(\frac{p_{cs}^{'}}{2}\right) = \frac{M}{2} \cdot \left(p_i^{'\left(\frac{\kappa^*}{\lambda^*}\right)} \cdot \left[p_p^{'}\frac{\eta_p^2 + M^2}{2M^2}\right]^{\left(\frac{\lambda^* - \kappa^*}{\lambda^*}\right)}\right) \qquad Eq.\ [37]$$

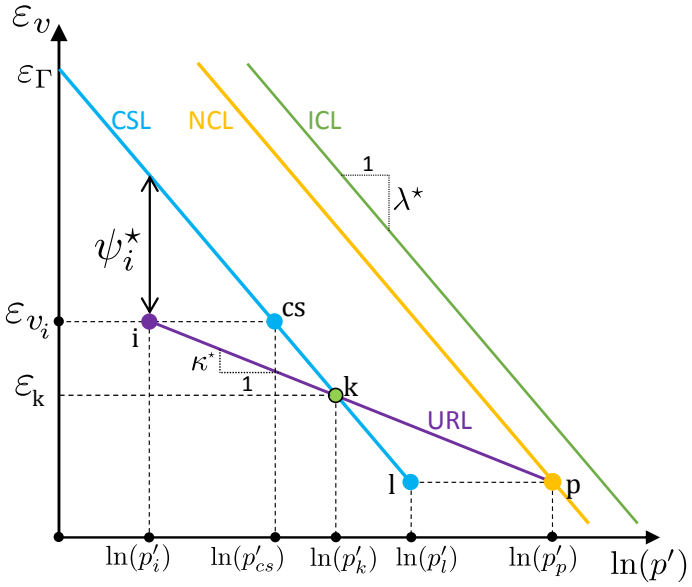

Figure 8: Schematic representation of isotropic consolidation line (ICL), NCL and CSL (after Wroth (1984))

List of state variables

Table 2: State variables

State parameter number	State variables name	Short description	Unit
1	init. flag	init. flag is used internally in the model to detect if the initialisation procedure has already been called. The initialisation of the model is executed at the beginning of the calculation, change of material or if **Reset state variables** is chosen in Phases settings menu in PLAXIS Input.	-
2	N/A	This state variable is currently not in use.	-
3	ε_{xx}	Total strain ε_{xx} used in small-strain stiffness calculations.	-
4	ε_{yy}	Total strain ε_{yy} used in small-strain stiffness calculations.	-
5	ε_{zz}	Total strain ε_{zz} used in small-strain stiffness calculations.	-
6	ε_{xy}	Total strain ε_{xy} used in small-strain stiffness calculations.	-
7	ε_{yz}	Total strain ε_{yz} used in small-strain stiffness calculations.	-
8	ε_{zx}	Total strain ε_{zx} used in small-strain stiffness calculations.	-
9	G^{ref}	Current reference shear modulus G^{ref} (used in small-strain stiffness calculations).	stress
10	G/G_{ur}	Current ratio between tangential shear modulus G and elastic unloading-reloading shear modulus G/G_{ur} (used in small-strain stiffness calculations).	-
11	ε_{vt}	Current volumetric total strain.	-
12	initial σ_3'	Minor principal stress at the initialisation phase.	stress
13	initial p'	Mean effective stress at the initialisation phase.	stress
14	ε_{Γ}	Intercept of the critical state line with ε_{vt} axis at the mean effective stress of p'=1 stress unit). At the initialisation phase ε_{Γ} is calculated from the given initial stress state and the pre-consolidation stress p_p' which is evaluated via parameters K_0^{nc} and *POP*.	-
15	$\bar{\psi}^*$	Modified conjugate state parameter as defined in Eq. 15.	-

State parameter number	State variables name	Short description	Unit
16	ψ^*	Modified state parameter as defined in Eq. 14.	-
17	R	Over-consolidation ratio.	-
18	ω	Hardening coefficient as defined in Eq. 17.	-
19	p_0	Yield surface intercept with p' axis.	stress
20	$\bar{p}_0$	Bounding surface intercept with p' axis.	stress

5

Calculation of PLAXIS parameters and Model Calibration

Calculation of PLAXIS Parameters

To show the applicability of the model within PLAXIS Soil Test and the resulting mechanical performance, the model parameters calibrated for London Clay by Jockovic and Vukicevic (2017) (on page 37) have been considered in this section. These parameters have been selected upon the experiments performed by Gasparre (2005) (on page 37) (*Table 3*) and they are used with the purpose of calculating the set of parameters required in PLAXIS input (*Table 5*). Heareafter, a detailed description about how to calculate these parameters is presented:

Table 3: Material parameters calibrated by Jockovic & Vukicevic (2017) for London clay

Parameters	λ	κ	M	Γ	ν_{ur}
London clay	0.168	0.064	0.80	2.85	0.2

- For the sake of simplicity, the same value of the initial specific volume is chosen for all the samples (i.e., $v_i^{ref} = 1 + e_i^{ref} = 1.954$) to calculate λ^* and κ^*. This specific value of $v_i = 1.954$ is here considered as a reference value through which the slope of the *CSL* and the *URL* (i.e., $v_i^{ref} = 1.954$) are calculated:

$$\lambda^* = \frac{\lambda}{v_i^{ref}} = 0.086, \quad \kappa^* = \frac{\kappa}{v_i^{ref}} = 0.033$$

- If p^{ref} is taken to be equal to *100kPa*, it is possible to obtain the following values for E_{ur}^{ref} and E_{oed}^{ref}, by applying Eq. 25:

$$E_{ur}^{ref} = \frac{p^{ref}\ 3\left(1 - 2\,\nu_{ur}\right)}{\kappa^*} = 5496\ kPa, \quad E_{oed}^{ref} = \frac{p^{ref}}{\lambda^*} = 1163\ kPa$$

- The friction angle at critical state φ_{cs} can be obtained through the definition of *M* which represents the slope of the critical state conditions in the plane *p-q*:

$$\varphi_{cs} = arcsin\left[\ \frac{3M}{6 + M}\ \right] = 20.7^\circ$$

- Due to the isotropic initial conditions, K_0^{nc} has been selected equal to K_0^{nc}=1.

- To avoid the small strain stiffness framework G_0^{ref} and $\gamma_{0.7}$ have been selected equal to $G_0^{ref} = \gamma_{0.7} = 0$.
- To calculate the Pre-Overburden Pressure *(POP)*, Eq. 29 can be rearranged as:

$$POP = p_p^{'}\left(\frac{3}{1+2K_0^{nc}}\right) - \sigma_{v0}^{'} = p_p^{'} - \sigma_{v0}^{'} = p_p^{'} - p_i^{'}$$

In which $p_p^{'} = 2p_k^{'}$ and $K_0^{nc} = 1$ due to isotropic initial condition. $\sigma_{v0}^{'}$ is the initial vertical effective stress, which for the case an initial isotropic state is equal to $p_i^{'}$.

The variable $p_k^{'}$, can be obtained by enforcing the same specific volume at the intersection between the *URL* and *NCL*:

$$v_\kappa^{csl} = \Gamma - \lambda \ln\left(p_k^{'}\right) = v_\kappa - \kappa \ln\left(p_\kappa^{'}\right) = v_\kappa^{url} \qquad Eq.\ [38]$$

Which enables to express $p_k^{'}$ as:

$$p_\kappa^{'} = exp\left(\frac{v_\kappa - \Gamma}{\kappa - \lambda}\right) \qquad Eq.\ [39]$$

Where the specific volume v_κ at the intersection between *CSL* and *URL* can be calculated from the initial value of the specific volume v_i:

$$v_\kappa = v_i + \kappa \ln\left(p_i^{'}\right) \qquad Eq.\ [40]$$

By combining Eq. 39 and Eq. 40:

$$p_k^{'} = exp\left(\frac{v_i + \kappa \ln\left(p_i^{'}\right) - \Gamma}{\kappa - \lambda}\right) \qquad Eq.\ [41]$$

In this manner, the *POP* can be calculated in terms of the initial conditions of the material after consolidation $p_i^{'}$:

$$POP = 2 \cdot exp\left(\frac{v_i + \kappa \ln\left(p_i^{'}\right) - \Gamma}{\kappa - \lambda}\right) - p_i^{'} \qquad Eq.\ [42]$$

The intermediate variables employed to calculate *POP* for London Clay corresponding to different values of the *OCR* are reported in *Table 4*, while in *Table 5* it is shown the list of parameters used in Soil Test calculations:

Table 4: List of variables calculated to obtain *POP* for different values of the Over-Consolidation Ratio

Sample ID	OCR=20	OCR=2.25	OCR=1
$p_i^{'}$ [kPa]	30	200	317
v_i [-]	2.040	1.954	1.952
v_κ [-]	2.258	2.293	2.321
$P_k^{'}$ [kPa]	297.5	211.6	162.5

Sample ID	OCR=20	OCR=2.25	OCR=1
$P_p^{'}$ [kPa]	595.0	423.3	325
POP [kPa]	565.0	223.3	8.0

Table 5: Input parameters employed in PLAXIS calculations (calculated from Table 3).

Parameter	Value	Unit
E_{ur}^{ref}	5496	$\mathrm{kN/m^2}$
υ_{ur}	0.2	-
E_{oed}^{ref}	1163	$\mathrm{kN/m^2}$
p^{ref}	100	$\mathrm{kN/m^2}$
G_0^{ref}	0	$\mathrm{kN/m^2}$
$\gamma_{0.7}$	0	-
φ_{cs}	20.7	o
K_o^{nc}	1	-
POP	565	$\mathrm{kN/m^2}$
h	1	-

It is worth remarking that by observing *Table 4*, there is a discrepancy between the value of *POP* and the normal consolidated state of the soil. As a matter of fact, the *POP* corresponding to *OCR*=1 should vanishe due to the equivalence between the maximum and current stress state (i.e., $\sigma_v^{',max} = \sigma_v^{'}$) while the value calculated by means of Eq. 42 is equal to *POP*=8 *kPa*. This mismatch between the theoretical value of *POP* and the corresponding value calculated through a prescribed initial state (i.e., p_i and υ_i) is explained by a small drift on υ_i with respect to the reported value p_i. Despite this inconsistency, the level of over-consolidation is small enough so it is still possible to consider the *OCR* close to one.

The model performance has been studied by computing the material response through a set of undrained triaxial tests at different values of the *POP* (i.e., a different value of the over-consolidation ratio *OCR*). These analyses have been performed with PLAXIS Soil Test and the results are plotted in *Figure 9* and *Figure 10*.

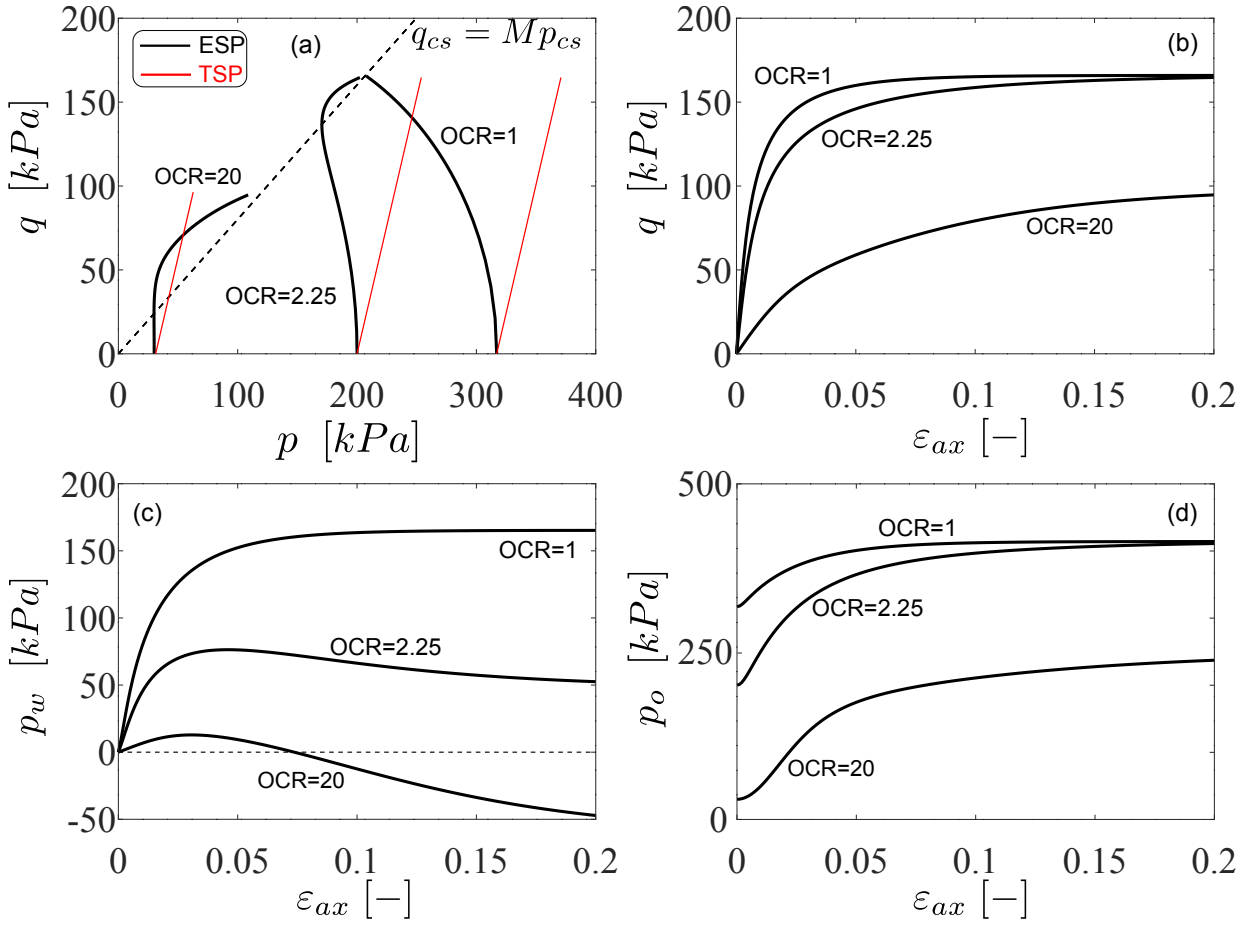

Figure 9: Stress paths in q-p' plane and stress-strain curves in q-ε_{ax} plane for 3 samples of London clay having different initial over-consolidation ratios

Specifically, in *Figure 9(a)* it is possible to observe the transition of the stress path from the characteristic normal consolidated behaviour (i.e., *OCR*=1) to the S-shaped response of a highly over-consolidated clay (i.e., *OCR*=20). The tendency of the material to dilate can be observed in *Figure 9 (c)* where the excess pore pressure is plotted for the different values of the over consolidated ratio (i.e., *OCR*=1, *OCR*=2.25 and *OCR*=20) as a function of the axial strains. This trend of behaviour tends to be more accentuated for increasing values of the *OCR* for which negative increments of pore pressure are cumulated. In all these cases, the material tends to reach a critical state at the end of the loading.

It is worth remarking that the model prediction with *OCR*=1 corresponds to the classical response of Modified Cam-Clay model as *R* and ω are equal to one (*Figure 10*).

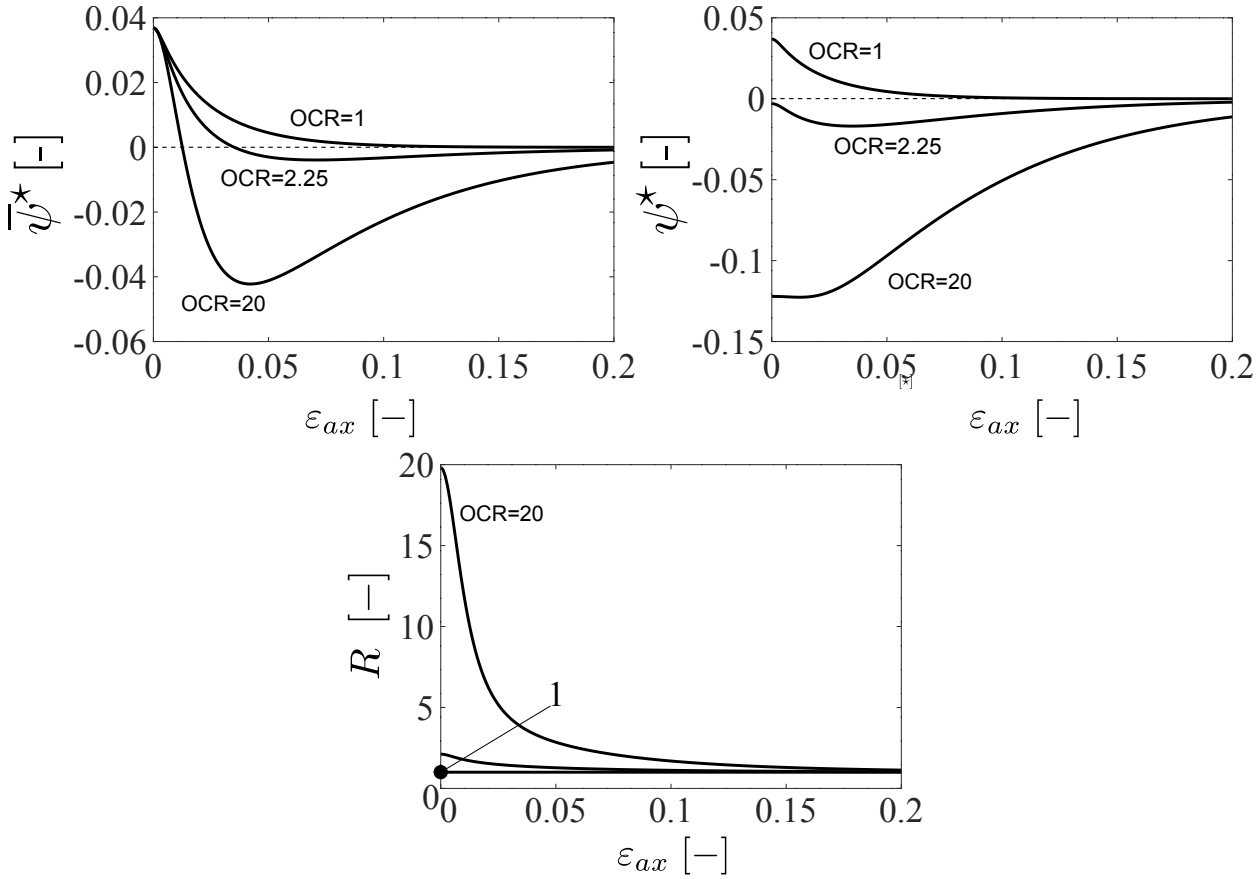

Figure 10: Evolution of the state parameters ψ^*, $\bar{\psi}^*$, and the overconsolidation ratio R during the undrained compressions reported in Figure 9

Parameter h

To guarantee more flexibility in calibrating stress paths resulting from laboratory experiments, a parameter *h* has been introduced in the hardening rule, through the hardening parameter ω (Eq.17). Although this parameter is not associated to a specific physical meaning, its purpose is to magnify or reduce the volumetric hardening during the loading process, thus enabling a better calibration of a *GIVEN* stress path. An example of this logic is shown in *Figure 11* to *Figure 13* in which the drained and undrained triaxial compression path have been performed on a highly over-consolidated sample tested with different values of the parameter *h*.

The results emphasize the effect on the stress path when selecting decreasing values of *h* (*Figure 11(a)-(b)*). In particular, small values of *h* accentuates the S-shaped response in undrained conditions due to its limited variation of the increment of the hardening variable $\dot{p}_0$. As reported in *Figure 11 (a)*, *h*=0.001 represents a lower bound, below which no effect on the stress path is observed. On the contrary, the effect of increasing the value of *h*, as illustrated in *Figures 11(c)-(d)*, results in an augmented capability to cumulate negative pore pressures. This tendency is plotted in *Figure 12* where the evolution of the pore pressures is reported for different values of the parameter *h*. The same parametric analyses have been performed also by testing drained triaxial stress paths and they are shown in *Figure 13.*

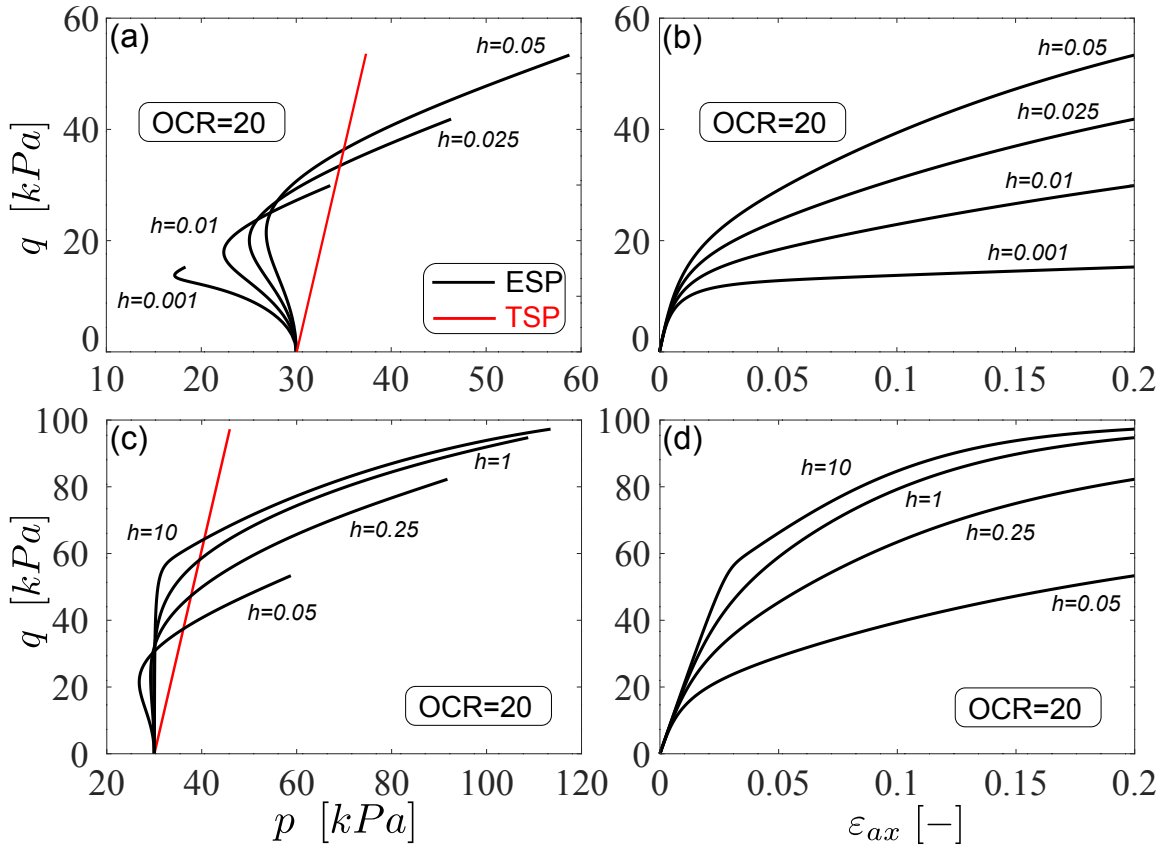

Figure 11: Stress paths in q-p' plane and stress-strain curves in q-ε_{ax} plane for 3 samples of London clay with the same initial over-consolidation ratios and different values of the parameter h

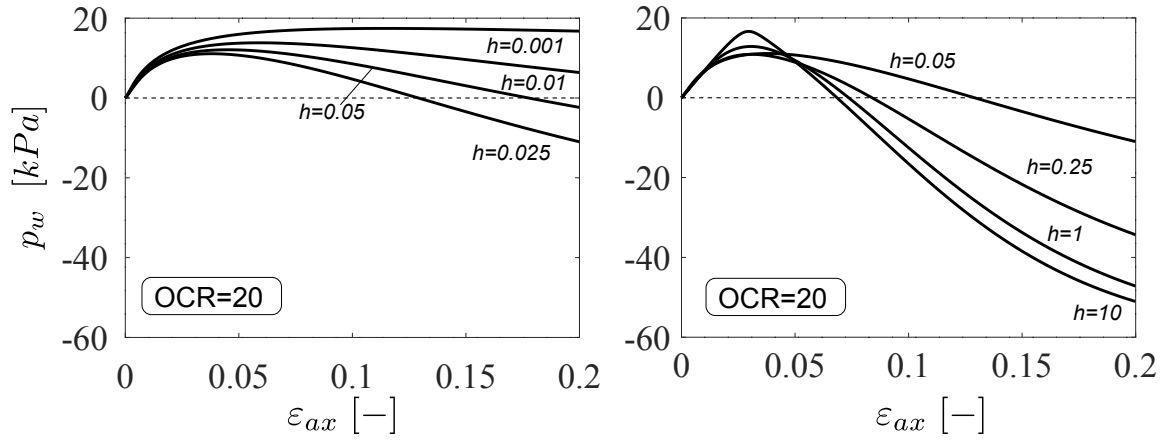

Figure 12: Evolution of the excess of pore pressure p_w corresponding to different values of the parameter h at the same initial over-overconsolidation ratios. the parameters listed in Table 3 to Simulate the London Clay are considered.

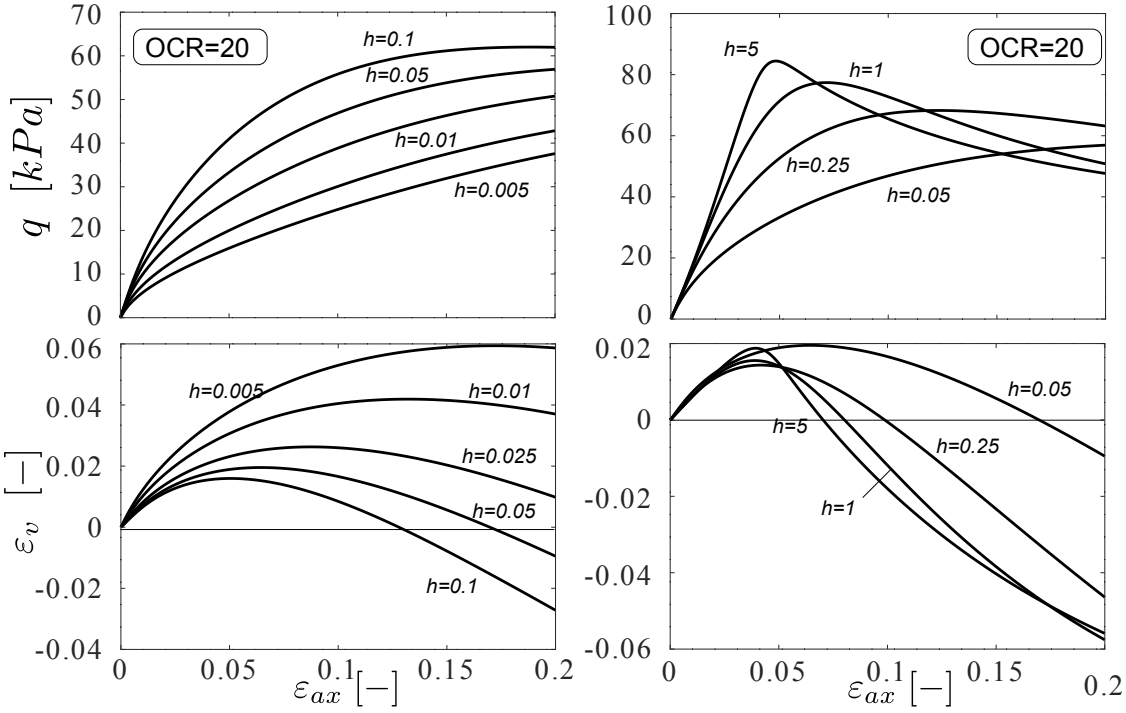

Figure 13: Mechanical response obtained by computing a drained stress path for different values of the parameter h

Model calibration

A calibration of different clays is detailed in the following sections to inspect the capabilities of the *HASP* model.

London clay

The parameters employed to simulate London Clay are the reported in *Table 5*.

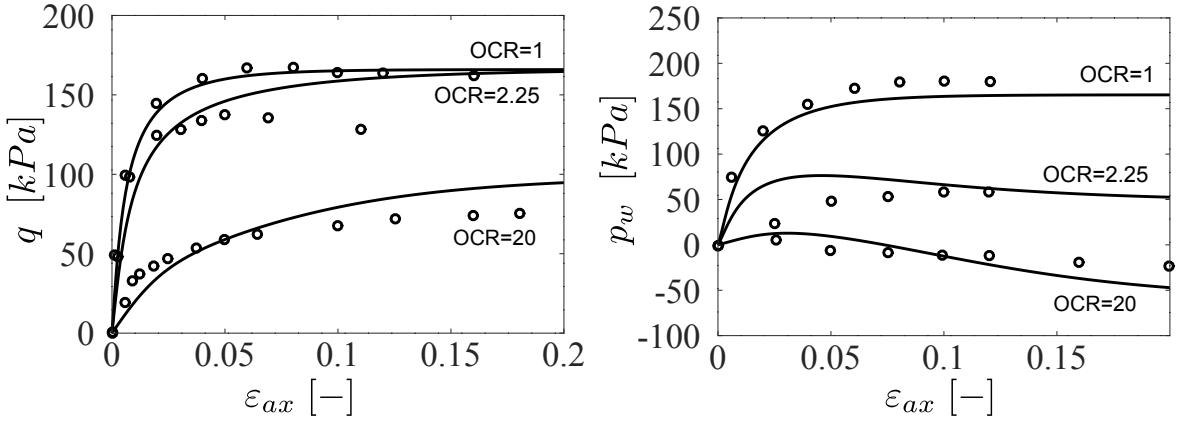

Figure 14: Model calibration of undrained triaxial stress paths of London Clay for different values of the over-consolidated ratio

Cardiff Clay

The parameters used to model Cardiff Clay are reported in *Table 6* to *Table 8* . To calculate the elastic properties a reference specific volume v_i^{ref} equal to v_i^{ref} =1.947 has been considered.

Table 6: Material parameters calibrated by Jockovic & Vukicevic (2017) for Cardiff clay

Parameters	λ	κ	M	Γ	v_{ur}
Cardiff clay	0.14	0.05	1.05	2.63	0.2

Table 7: List of variables calculated to obtain *POP* for different values of the Over-Consolidation Ratio

Sample ID	OCR=12	OCR=8	OCR=5
$p_i^{'}$ [kPa]	34.5	48.2	73
v_i [-]	1.973	1.963	1.947
v_κ	2.15	2.16	2.16
$P_k^{'}$ [kPa]	207	192	182
$P_p^{'}$ [kPa]	414	384	365
POP [kPa]	380	336	291

Table 8: Input parameters employed in PLAXIS calculations (calculated from Table 6).

Parameter	Value	Unit
E_{ur}^{ref}	7010	kN/m^2
v_{ur}	0.2	-
E_{oed}^{ref}	1390	kN/m^2
p^{ref}	100	kN/m^2
G_0^{ref}	0	kN/m^2

Parameter	Value	Unit
$\gamma_{0.7}$	0	-
φ_{cs}	28.4	o
K_0^{nc}	1.0	-
h	0.5	-

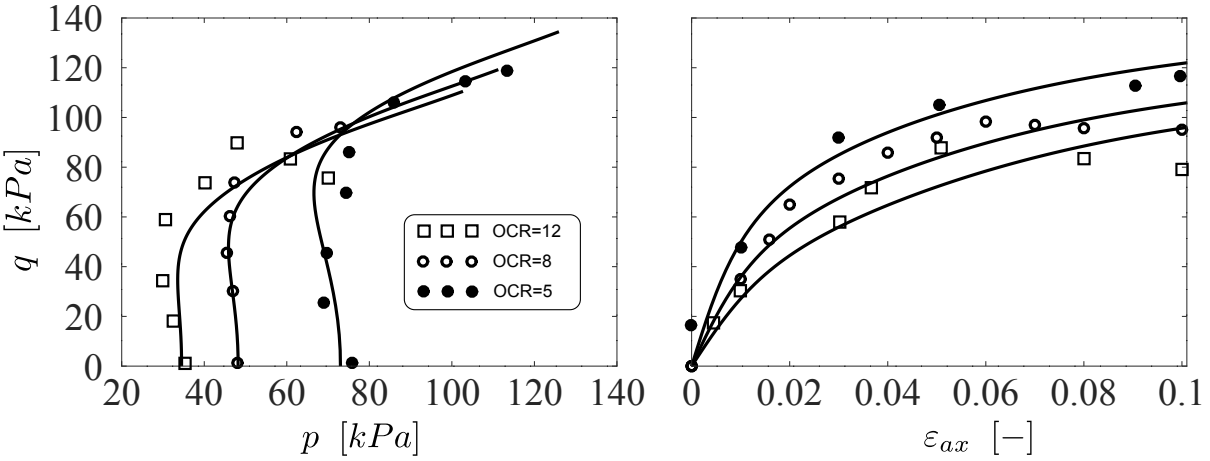

Figure 15: Stress paths in q-p' plane and stress-strain curves in q-ε_{ax} plane for 3 samples of Cardiff clay having different initial over-consolidation ratios

Bangkok clay

The parameters used to model Bangkok Clay are reported in *Table 9* to *Table 11*. To calculate the elastic properties a reference specific volume v_i^{ref} equal to v_i^{ref} =2.24 has been considered without explicitly detailing the intermediate variables calculated to obtain *POP* as done in *Table 4* and *Table 7*.

Table 9: Material parameters calibrated by Jockovic & Vukicevic (2017) for Bankok clay

Parameters	λ	κ	M	Γ	ν_{ur}
Bankok clay	0.1	0.02	1.13	2.85	0.2

Table 10: List of variables calculated to obtain *POP* for different values of the Over-Consolidation Ratio

Sample ID	OCR=24	OCR=8	OCR=2	OCR=1.5
$p_i^{'}$ [kPa]	34	103	414	552
v_i [-]	2.3	2.275	2.245	2.24

Sample ID	OCR=24	OCR=8	OCR=2	OCR=1.5
POP [kPa]	768	728	439	294

Table 11: Input parameters employed in PLAXIS calculations (calculated from Table 9).

Parameter	Value	Unit
E_{ur}^{ref}	40320	$\mathrm{kN/m^2}$
υ_{ur}	0.2	-
E_{oed}^{ref}	4480	$\mathrm{kN/m^2}$
p^{ref}	100	$\mathrm{kN/m^2}$
G_0^{ref}	0	$\mathrm{kN/m^2}$
$\gamma_{0.7}$	0	-
φ_{cs}	28.4	o
K_0^{nc}	1.0	-
h	1	-

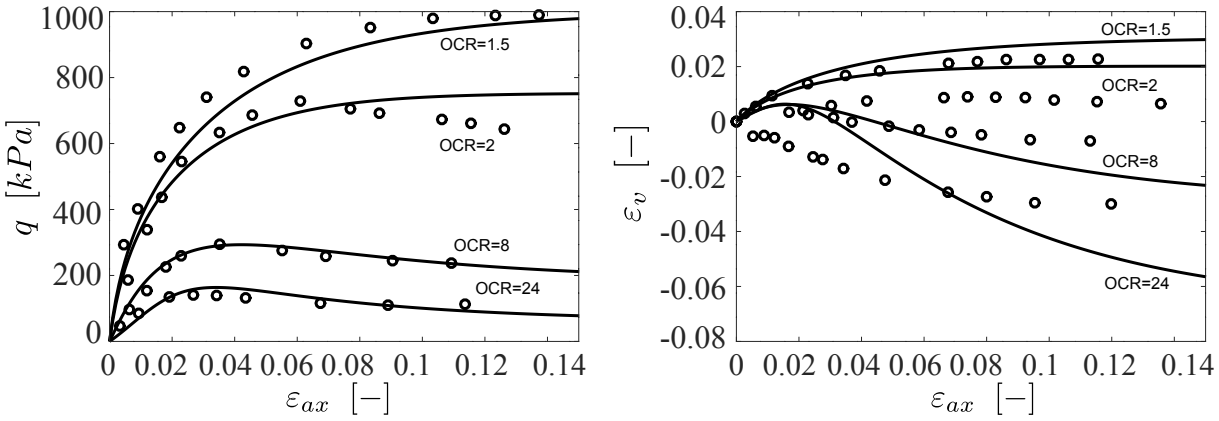

Figure 16: Model Calibration of Bangkok Clay by comparing the numerical results with drained triaxial tests performed are different OCR

Black Kaolin clay

The parameters used to model Black Kaolin Clay are reported in *Table 12* to *Table 14* . To calculate the elastic properties a reference specific volume v_i^{ref} equal to v_i^{ref} =2.07 has been considered. The initial conditions and the *POP* values, corresponding to different degrees of overconsolidation, are listed in *Table 13*.

Table 12: Material parameters calibrated by Jockovic & Vukicevic (2017) for Kaolin clay

Parameters	λ	κ	M	Γ	v_{ur}
Kaolin clay	0.23	0.03	0.81	3.44	0.2

Table 13: List of variables calculated to obtain *POP* for different values of the Over-Consolidation Ratio

Sample ID	OCR=2	OCR=4	OCR=8
$p_i^{'}$ [kPa]	400	200	100
v_i [-]	2.09	2.07	2.05
POP [kPa]	756	652	449

Table 14: Input parameters employed in PLAXIS calculations (calculated from Table 12).

Parameter	Value	Unit
E_{ur}^{ref}	12420	kN/m^2
v_{ur}	0.2	-
E_{oed}^{ref}	900	kN/m^2
p^{ref}	100	kN/m^2
G_0^{ref}	0	kN/m^2
$\gamma_{0.7}$	0	-
φ_{cs}	21	o
K_0^{nc}	1.0	-
h	1	-

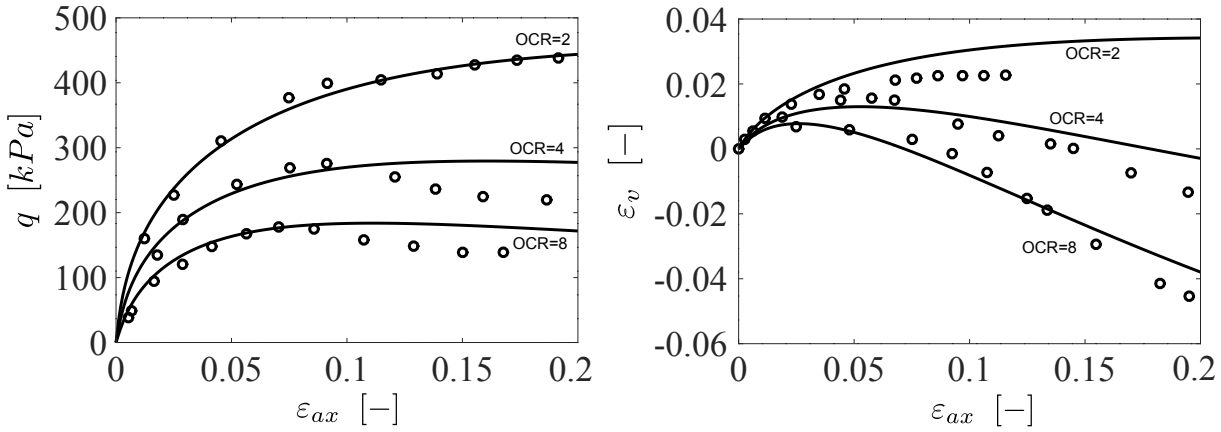

Figure 17: Stress paths in q-p' plane and stress-strain curves in q-ε_{ax} plane for 3 samples of Black kaolin clay having different initial over-consolidation ratios

6
Finite Element Analyses with PLAXIS

The performance of the model is further tested by solving three different boundary value problems: a pressuremeter test, a retaining wall problem and a tunnel excavation. In these computations the parameters of small strain overlay model are employed for an accurate prediction of the soil deformability.

Pressuremeter test

To improve the material parameters proposed for London Clay, a further calibration is proposed in this section where the model parameters have been optimized on the basis of the results obtained from a pressuremeter test performed at 28 meter of depth in London Area. Due to the low permeability of London Clay undrained conditions have been considered. A sketch of the initial and boundary conditions employed in PLAXIS code are depicted in *Figure 18 (a)* in which the result of the test expressed in terms of total pressure as a function of the imposed radial displacements have been also reported (*Figure 18 (b)*). As shown in *Figure 18 (b)*, the test includes three different cycles of loading/reloading, two in the initial loading branch and one in the unloading part of the test.

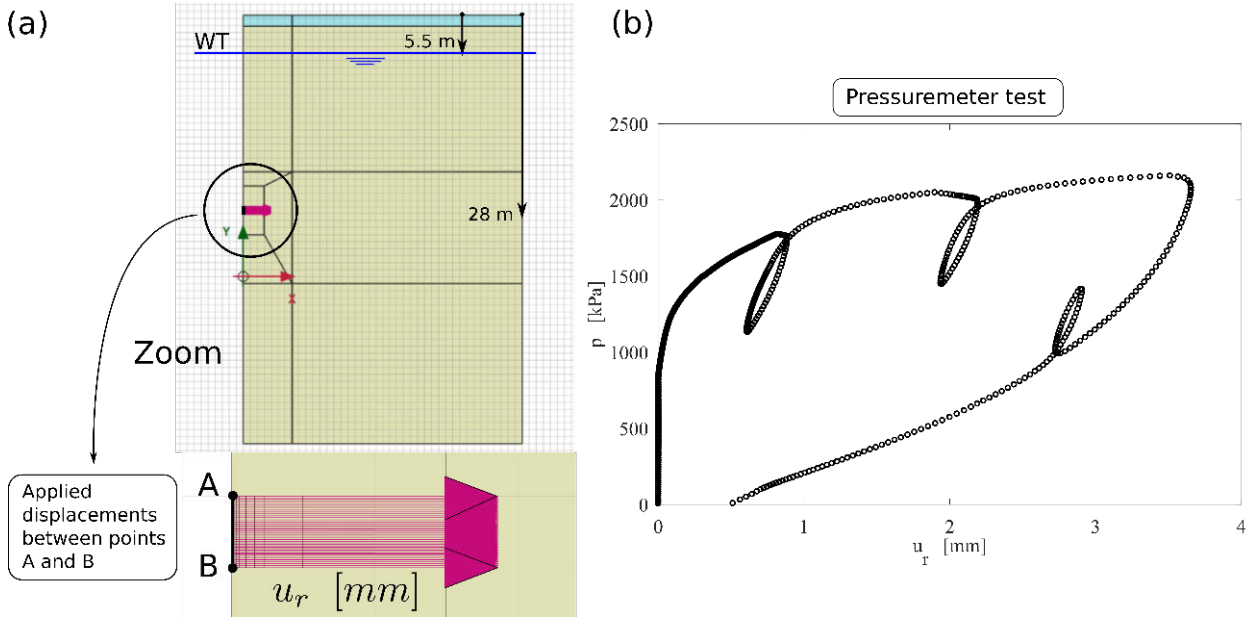

Figure 18: (a) Sketch of the Initial Boundary Value Problem solved to model the pressuremeter test in London Clay, (b) Experimental data after the pressure-meter test (after Salas, 2019)

According with the geological characterization of London Clay deposit (Hight, 2003 (on page 37)), the erosion of a remarkable layer of sediments is the main geological process resulting to a strong over-consolidation effect of the clay. The height of the eroded soil layer between Essex and Wraysbury district varies from 150 m to 300 m. In the specific area where the pressuremeter test has been performed, a pre-overburden *POP*=2000 *kPa* is considered (Salas, 2019 (on page 37)), which corresponds to a height of the eroded soil of 200 m. A first set of computations have been performed with the set of parameters reported in *Table 15* which includes also the parameters reported in *Table 5* except for the parameter used to describe small strain framework (i.e., G_0^{ref} and $\gamma_{0.7}$).

Table 15: Input parameters used in Figure 17 for the numerical modeling of the pressuremeter test. The parameters SIM 1 are the ones proposed by Gasparre (2005)

SIM 1	v_{ur}	p^{ref}	λ	e_0	λ^*	E_{ur}^{ref}	κ	κ^*	E_{oed}^{ref}	G_0^{ref}	$\gamma_{0.7}$	φ_{cs}	K_0^{nc}	POP
	[-]	[kPa]	[-]	[-]	[-]	[kPa]	[-]	[-]	[Pa]	[MPa]	[-]	[°]	[-]	[kPa]
1	0.2	100	0.09	0.7	0.05	6460	0.05	0.0279	1890	42.5	3.1×10^{-4}	25.4	0.6	2000
2			0.1	0.95	0.05	35172	0.01	0.0051	1954					
3			0.168	0.95	0.09	5496	0.064	0.0328	1163					

The results are reported in *Figure 19* in which the three different lines correspond to the three different set of parameters listed in *Table 15* (*h*=1 is considered in all the cases). The green line is the curve closer to the experimental results and corresponds to the parameters proposed in Gasparre (2005) (on page 37). This set of parameters (SIM1), is also considered to study the effect of *h* on the loading/reloading process of the pressuremeter.

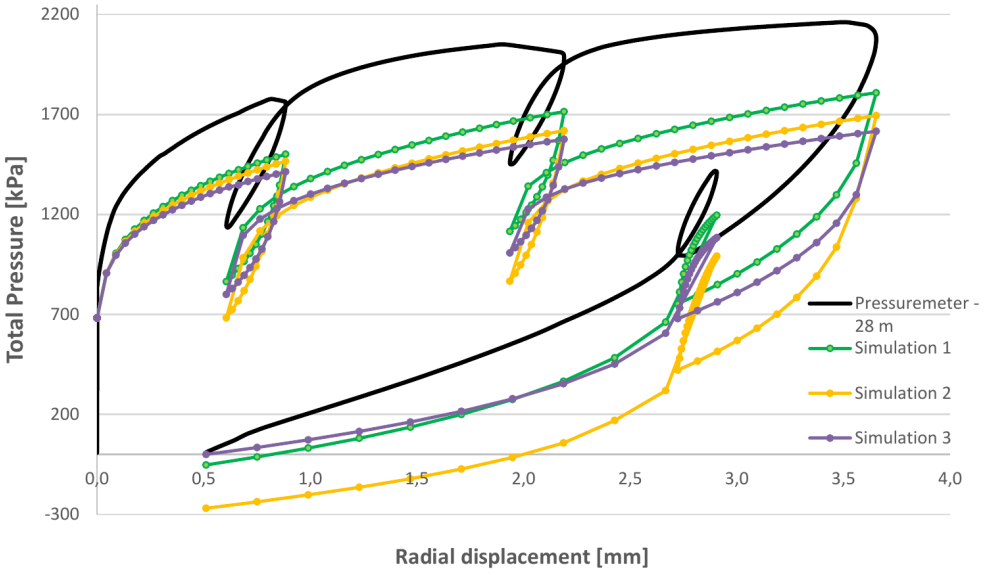

Figure 19: Numerical modeling of the pressuremeter for the parameters reported in Table 15 (after Salas, 2019)

By considering the parameters referred to as SIM 1 in *Table 15*, four different values of h (i.e., *h*=1.0, *h*=1.5, *h*=5 and *h*=10) which correspond respectively to the simulations 1, 2, 3, and 4) have been tested. The results are shown in *Figure 20* and they emphasize how the model response approaches the experimental results. A further computation has been added in *Figure 20* (pink curve corresponding to Simulation 5). For this curve a value *h*=10 has been considered and the parameters of the small strain model changed to G_0^{ref} =82.6, $\gamma_{0.7}$=1.3x10^{-4} (after Salas, 2019 (on page 37)).

Consistently with the results reported in *Figure 11*, *Figure 12* and *Figure 13*, an increase of the parameter *h* result to a stiffer response of the soil.

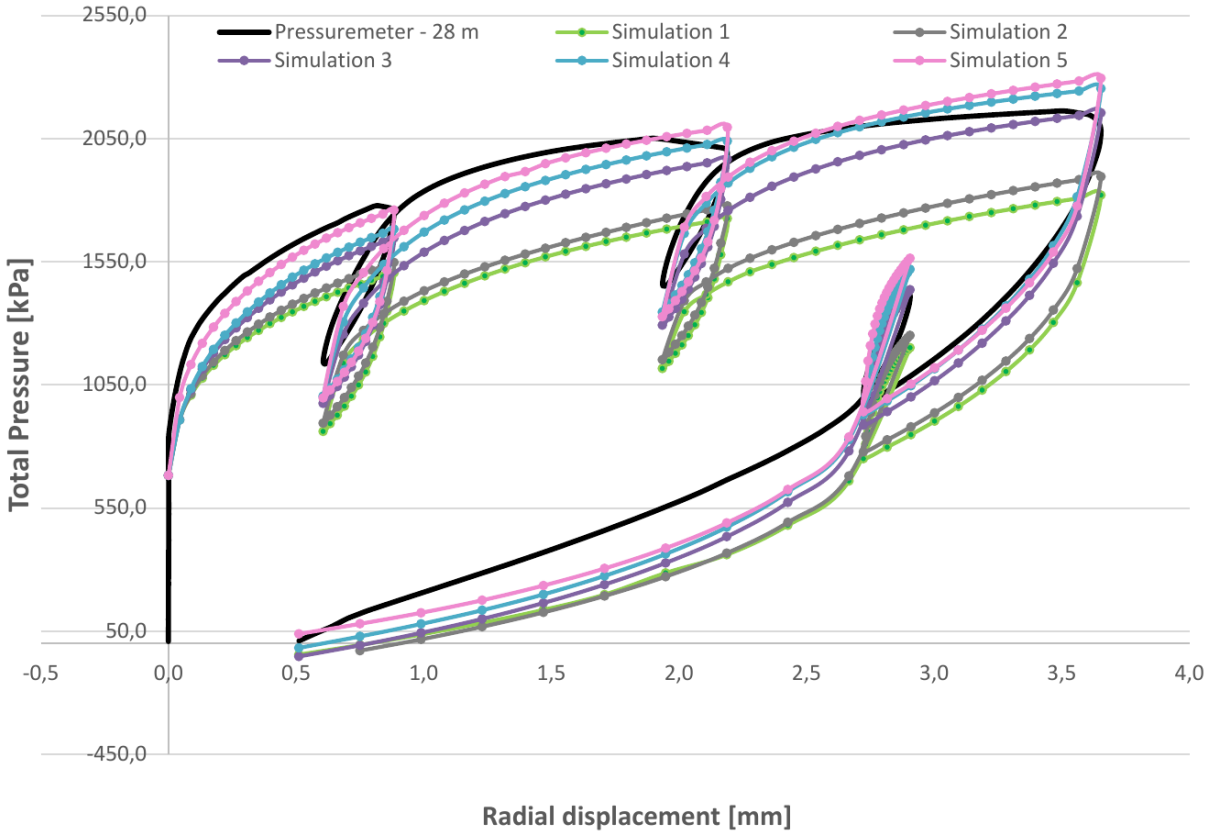

Figure 20: Numerical modeling of the pressuremeter test for the parameters reported in Table 15, SIM1. The pink curve corresponds to h=10, and the parameters of the small strain model equal to G_0^{ref} =82.6, $\gamma_{0.7}$=1.3x10-4 (after Salas, 2019)

The effect of a different loading/reloading behaviour as depicted in *Figure 5* is investigated through the pressuremeter test and the results are reported in *Figure 21*. To have an elastic reloading phase the input flag *elReload* is set to one. The same set of parameters employed to obtain the results illustrated in *Figure 20* are used in the computations presented in *Figure 21*. A zoom of the cycles performed with both strategies is also reported in this figure and emphasizes the difference of having a reloading phase within a plastic regime. While the unloading regime is characterized by the same trend of behaviour due to the same elastic behavior, in the reloading phase the material with a plastic behavior is less stiff than its counterpart in the elastic regime.

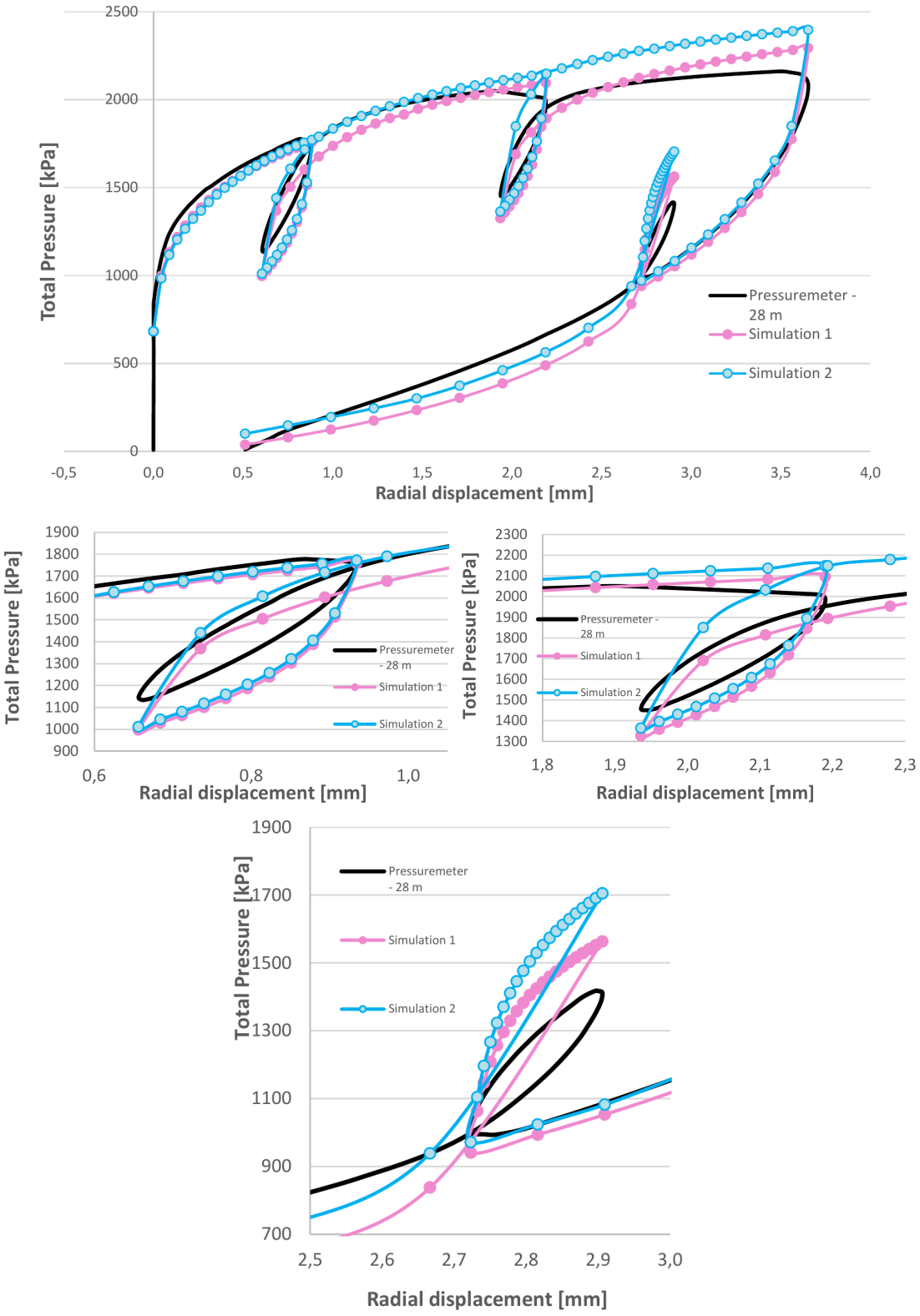

Figure 21: Numerical modeling for the pressure test using the parameters employed the green line in Figure 18 and by considering the different behaviour in loading and reloading (after Salas, 2019).

Acknowledgements

The validation of the *HASP* model has been carried out in collaboration with ARUP London and Imperial College. In particular, the research engineers of Plaxis BV want to thank Prof. Zdrakovic, Prof. Simpson, Dr. Pillai and J. Salas for their work and useful discussions regarding the numerical testing of the model with PLAXIS code.

7
References

1. Atkinson, J. and Sallfors, G. (1991). Experimental determination of soil properties. Proceedings of the 10th ECSMFE, Florence, 3, pp.915-956
2. Benz, T. (2007). Small-strain stiffness of soils and its numerical consequences. Ph.D. Universität Stuttgart.
3. Casagrande, A. (1936). The determination of pre-consolidation load and its practical significance, Discussion D-34. Proceedings of the 1st International Conference on Soil Mechanics and Foundation Engineering, Cambridge, 3, pp.60-64.
4. Chen, Y. and Yang, Z. (2017). A family of improved yield surfaces and their application in modeling of isotropically over-consolidated clays. Computers and Geotechnics, 90, pp.133-143.
5. Gao, Z., Zhao, J. and Yin, Z. (2017). A Dilatancy Relation for Overconsolidated Clay. International Journal of Geomechanics, 17(5), p.20.
6. Gasparre (2005). Advanced laboratory characterization of London Clay. Ph.D. thesis, Imperial College of London, London, UK.
7. High, D.W., McMillan, F., Powell J.J.M., Jardine, R. J., Allenou, C. P., (2003). Some characteristics of London Clay. Characterisation and Engineering Properties of natural soils- Tan et el. (eds) 2003 Swets & Zeitlinger, Lisse, ISBN 9058095371.
8. Hueckel, T. , Tutumluer, E. and Pellegrini, R. (1992), A note on non-linear elasticity of isotropic overconsolidated clays. Int. J. Numer. Anal. Meth. Geomech., 16: 603-618.
9. Jocković, S. and Vukićević, M. (2017). Bounding surface model for overconsolidated clays with new state parameter formulation of hardening rule. Computers and Geotechnics, 83, pp.16-29.
10. Mita K. A., Dasari G. R., Lo K. W. Performance of a three-dimensional Hvorslev-modified Cam-Clay model for overconsolidated clay. Int. J. Geomech. 2004;4:296-309.
11. Mitchell, J. and Soga, K. (2005). Fundamentals of Soil Behavior. 3rd ed. Hoboken (New Jersey): John Wiley & Sons, Inc., pp.400-402.
12. Nova R. (2006), Modelling of bonded soils with unstable structure. In: International workshop on modern trends in geomechanics - Vienna. Springer 2006.
13. Nova R., Wood D. M., (1979) A constitutive model for sand in triaxial compression. Int. J. Numer. Anal. Meth. Geomech.; 3: 255-278.
14. Pender, M. (1978). A model for the behaviour of overconsolidated soil. Géotechnique, 28(1), pp.1-25.
15. Salas, Jorge (2019). Validation of a constitutive model for overconsolidated clays. MSc Thesis, Faculty of Engineering, Imperial College London (in collaboration with Arup London, UK).
16. van Eekelen, H.A.M (1980). Isotropic yield surfaces in three dimensions for use in soil mechanics. International Journal for Numerical and Analytical Methods in Geomechanics, 4(1), 89-101 .
17. Vucetic, M. and Dobry, R. (1991). Effect of Soil Plasticity on Cyclic Response. Journal of Geotechnical Engineering, 117(1), pp.89-107.
18. Whittle AJ., Evaluation of a constitutive model for overconsolidated clays. Géothechnique 1993; 43: 289-313
19. Wroth C. P. (1984). The interpretation of in situ soil tests. Géotechnique 34, 4: 449-489

References

20. Yao, Y., Hou, W. and Zhou, A. (2009). UH model: three-dimensional unified hardening model for overconsolidated clays. Géotechnique, 59(5), pp.451-469.

21. Yao, Y., Hou, W. and Zhou, A. (2008). Constitutive model for overconsolidated clays. Science in China Series E: Technological Sciences, 51(2), pp.179-191.